Applied Catalysis B: Environmental 100 (2010) 328–337

Contents lists available at ScienceDirect

Applied Catalysis B: Environmental

journal homepage: www.elsevier.com/locate/apcatb

Electrochemical promotion of Pt(1 1 1)/YSZ(1 1 1) and Pt–FeO_x/YSZ(1 1 1) thin catalyst films: Electrocatalytic, catalytic and morphological studies

E. Mutoro[a,1], C. Koutsodontis[b], B. Luerssen[a], S. Brosda[b,*], C.G. Vayenas[b], J. Janek[a]

[a] Institute of Physical Chemistry, Justus-Liebig-University Giessen, Heinrich-Buff-Ring 58, 35392 Giessen, Germany
[b] Department of Chemical Engineering, University of Patras, Caratheodory St 1, 26500 Patras, Greece

ARTICLE INFO

Article history:
Received 4 June 2010
Received in revised form 28 July 2010
Accepted 5 August 2010
Available online 13 August 2010

Keywords:
Electrocatalysis
EPOC
Ethylene oxidation
Iron additives
Morphology
NEMCA
Platinum
PLD
Spillover
YSZ

ABSTRACT

The electrochemical promotion of ethylene oxidation on Pt was investigated using Pt(1 1 1) thin film model catalyst–electrodes deposited on top of YSZ(1 1 1) single crystals. This is the first study involving a thin epitaxial and well-characterized catalyst system. The nearly covering Pt films were prepared by pulsed laser deposition (PLD) and characterized by scanning electron microscopy (SEM), energy dispersive X-ray spectroscopy (EDX), and X-ray diffraction (XRD). In order to explore the influence of potentially catalytic active impurities, samples with and without FeO_x dopants on the Pt catalyst surface were investigated. A major result is that most of the samples showed unequivocal electrochemical promotion of catalytic activity (EPOC). The Faradaic efficiency values Λ are typically 2.5–77 which is considerably smaller than those reported for usually investigated macroscopically porous paste electrodes ($\Lambda^{max} = 3 \times 10^5$). This fact can be attributed to the much shorter three-phase boundary (tpb) length of the catalyst films. The iron-doped samples showed a permanent effect (P-EPOC). The results are discussed in terms of morphology changes and iron-doping effects. A short survey of EPOC studies using different catalyst/electrolyte preparation techniques is given.

1. Introduction

1.1. Electrochemical promotion of catalysis

The catalytic activity of metal films in contact with solid electrolytes is strongly affected by applying electrical current or potential between the, usually porous, catalyst film (working electrode) and a counter electrode deposited on the solid electrolyte [1,2]. This phenomenon, known as electrochemical promotion of catalysis (EPOC) or non-Faradaic electrochemical modification of catalytic activity (NEMCA), is a very general observation as it has been investigated for more than 70 catalytic reactions on a number of catalysts (e.g. Pt, Pd, Rh, Ag, Au, Ni, IrO_2, RuO_2) and different conducting materials, like solid ion conductors (e.g. Y_2O_3-stabilized ZrO_2 (O^{2-}), β''-Al_2O_3 (Na^+), Nafion (H^+), CaF_2 (F^-)), mixed ionic–electronic conductors (e.g. TiO_2, CeO_2), aqueous or molten salt conductors. Work in this area has been reviewed [3–6].

Electrochemical promotion and single steps of the microscopic processes have been investigated by a number of (i) electrochemical techniques, including cyclic voltammetry (CV) [3,5,7,8], and electrochemical impedance spectroscopy (EIS) [3,5,9], (ii) catalytic techniques, including rate transient analysis [3] and work function measurements [2,3,5], and (iii) surface science techniques like X-ray photoelectron spectroscopy (XPS) [3,5,10–12], ultraviolet photoelectron spectroscopy (UPS) [11], temperature programmed desorption (TPD) [3,5,13], photoelectron emission microscopy (PEEM) [14,15], and scanning tunneling microscopy (STM) [3,16]. In addition, (iv) phenomenological analyses [17] and (v) theoretical ab initio quantum mechanical calculations [3,18,19] have been made. On the basis of these results EPOC has been attributed to the electrically controlled migration of a promoting spillover species, e.g. $O^{\delta-}$ from an oxygen ion conducting solid electrolyte to the catalytically active metal–gas interface [3–6].

The magnitude of electrochemical promotion is commonly described by two parameters, i.e. the rate enhancement ratio ρ, defined as:

$$\rho = \frac{r}{r_o} \quad (1)$$

* Corresponding author. Tel.: +30 2610 997576; fax: +30 2610 997269.
E-mail address: brosda@chemeng.upatras.gr (S. Brosda).
[1] Current address: Electrochemical Energy Laboratory, Massachusetts Institute of Technology, 77 Massachusetts Avenue, Cambridge 02139, USA.

0926-3373/$ – see front matter © 2010 Elsevier B.V. All rights reserved.
doi:10.1016/j.apcatb.2010.08.009

where r is the electropromoted rate and r_o is the open-circuit rate, and the Faradaic efficiency Λ, defined as:

$$\Lambda = \frac{r - r_o}{I/2F} = \frac{\Delta r}{I/2F} \quad (2)$$

where F is the Faradaic constant and I is the current. The term $I/2F$ corresponds to the rate of oxygen ions supplied to catalyst according to Faraday's law. Thus, $\Lambda = 1$ refers to a purely Faradaic rate enhancement.

More recently, a permanent EPOC (P-EPOC) has been observed for some systems, i.e. after stopping the polarization, the rate r does not drop to the initial value r_0 but to a higher one $r_{\text{P-EPOC}}$ [20]. In order to quantify this effect a parameter γ has been introduced as:

$$\gamma = \frac{r_{\text{P-EPOC}}}{r_o} \quad (3)$$

The majority of EPOC studies have been carried out using porous metal or metal oxide catalyst/electrode films prepared via calcination of metal dispersions in organic solvents (unfluxed pastes) [3–6]. However, in recent years a variety of other metal deposition techniques have been used, including sputtering [21,22], wet impregnation [23–26], thermal decomposition [27,28] or electrostatic spray deposition [29,30]. Appendix 1 provides a summary of published work including information on the catalyst system, the investigated reaction, and the observed ρ and Λ values.

1.2. Model-type catalysts

Using structurally, morphologically, geometrically and compositionally well-defined model-type catalysts, the complexity of the electrode/catalyst system is reduced. Additionally, this approach allows for the application of well established surface analytical techniques, which may contribute to characterize the occurring processes and strengthen the microscopic interpretation. However, these samples differ from real ones referring to the so-called "materials gap". Thus, the observation of an EPOC effect on well-defined model catalysts is an extremely important aspect, as it bridges this materials gap.

Up to now, there are only a few investigations on well characterized, single crystalline catalyst surfaces aiming for the identification of individual steps of EPOC, such as ex situ STM studies [3,16]. Using thin film Pt(1 1 1)/YSZ(1 1 1) electrodes like in this study, the spillover process has been imaged in situ by PEEM or SPEM [31,32]. However, these studies necessarily had not been carried out under real EPOC conditions, but under vacuum and without the presence of reactants. Anyway, this approach is promising to obtain deeper insights into the electrochemical processes occurring at polarized electrodes, especially if the pressure gap will be overcome in future by new in situ techniques like high pressure XPS. So far, an unequivocal surface spectroscopic identification of the chemical nature of the promoting surface oxygen species under in situ conditions (or better *in operando* conditions [33]) is still missing. Therefore, the demonstration of EPOC on model-type catalysts is a necessary step towards this aim.

1.3. Morphology

In previous EPOC studies little attention has been paid to the catalyst/electrode morphology and its possible modification during current and potential application. This is justified, as typical porous paste electrodes experience no or only modest morphology changes during operation due to a sufficient tpb length. However, using covering and gas-tight film electrodes involves a decreased tpb length which causes two differences: (i) Since oxygen – which is formed via anodic polarization – has to escape eventually to the gas phase, bubble formation can take place [32,34,35]. This morphology change has to be considered as an inherent disturbance of these kinds of model-type experiments. (ii) A small number of tpb sites – acting as the origin of $O^{\delta-}$ spillover – is expected to lead to a reduced electrochemical promotion (EPOC) compared to porous films.

1.4. Impurities

Like in every catalytic system, one may be concerned about the possible influence of impurities in the electrode system Pt|YSZ, particularly if such films are prepared by commercial platinum pastes on polycrystalline zirconia ceramics. For instance, a recent study of different types of electrodes showed that impurities, like Si, may have an effect on the shape of cyclic voltammograms of Pt|YSZ electrodes [35]. As CVs of Pt|YSZ electrodes have often been interpreted in terms of the oxygen spillover species [3,7,8], one might conclude from this observation that impurities may play an important role for the occurrence of EPOC. It is a central purpose of this paper to emphasize that this conclusion is not justified and to demonstrate that un-doped model-type Pt film electrodes having a sufficient tpb length show EPOC.

2. Experimental

2.1. Sample preparation

As working catalyst–electrodes different types of PLD model electrodes with and without iron (Fe) have been deposited on YSZ(1 1 1) single crystals (CrysTec, 1 cm × 1 cm × 0.1 cm, root-mean-square-surface-roughness of the polished side 0.160 nm). The iron-free films have been prepared as previously described [36]: laser wavelength 248 nm, laser energy about 450 mJ, 36,000 laser pulses, repetition rate 6 Hz, target-substrate distance 4.5 cm, temperature of 973 K corresponding to approximately 650 K on the substrate surface during ablation, and argon background gas (p = 1 Pa, purity 99.95%). For the Fe containing samples additionally 1000 pulses Fe were placed in the middle of the Pt film (pulse sequence: 18,000 Pt/1000 Fe/18,000 Pt), thus the average iron content is approximately 2.7%. The catalyst films covered about half (1.0 cm × 0.5 cm) of the substrate or the whole one respectively. Subsequent annealing in air was carried out either for 2 h at 1023 K (for Pt and Pt/Fe films) or 19 h at 1273 K for one Pt/Fe film. One pure Pt sample was additionally annealed for 14 h at 1473 K in order to increase the tpb length by a partial dewetting resulting in a few holes in the Pt film (sample Pt3 discussed below).

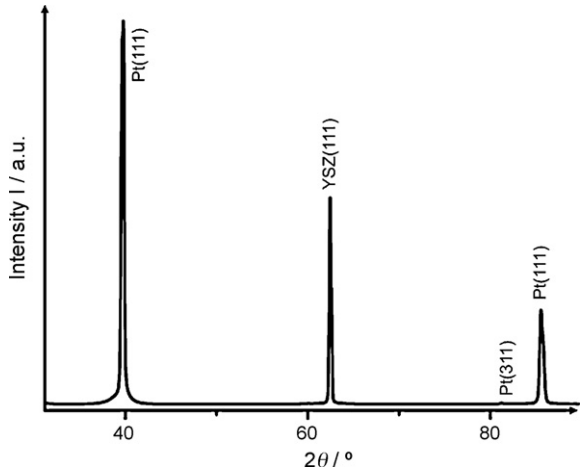

Fig. 1. Typical XRD of the catalyst films (covering Pt film before annealing; there are only minor differences due to iron doping, annealing, or the EPOC experiments).

Table 1
Sample notation, morphology, preparation details, geometric surface areas and an estimation of the tpb lengths before electrochemical polarization of the investigated catalyst–electrodes.

Notation	Morphology	Annealing temperature, T/K	Annealing time, t/h	Geometric surface area, A_G/cm^2	Estimated tpb length t_{tpb} of the sample/cm
Pt1	Covering	923	2	0.51	6.0
Pt2	Covering	923	2	0.56	6.2
Pt3	Partly porous	1273, 1473	19, 14	0.81	193.0
PtFe1	Covering	923	2	0.54	6.2
PtFe2	Covering	923	2	0.56	6.2
PtFe3	Covering	1273	19	0.98	7.6

The sample notation and preparation details of the six films used in this investigation are shown in Table 1, which also indicates their superficial geometric surface area (A_G) and a rough approximation of their tpb length (t_{tpb}) before the EPOC experiments. These values have been estimated by combining information on their microscopic (SEM images) and macroscopic geometry; e.g. the t_{tpb} of the electrode edges has been estimated as twice the macroscopic length due to their jagged structure (cp. Fig. 2a). It has been also assumed that there is no further roughness at the atomic scale which is, of course, not observable by the SEM images. Thus, the tpb length estimates of Table 1 represent only lower limits of the actual tpb length.

In a second step the counter and reference electrodes were placed both on the back of the electrolyte and sintered (723 K (heating rate 3 K/min) for 1 h, 973 K (heating rate 2 K/min) for 1 h). The sintering temperature was chosen to be at least 50 K lower than the annealing temperature of the catalyst–electrode in order to minimize any significant modifications of the catalyst–electrode morphology. Gold paste (Engelhard A1118) was chosen as the metal because the experiments were carried out in a single-chamber type reactor, and gold is known to be catalytically inactive in the temperature range of the kinetic investigation [3].

2.2. Electrode characterization

The catalyst films have been investigated by XRD (θ–2θ scans, Siemens Diffractometer D500/501) after annealing (Fig. 1). The morphology of the catalyst films has been studied by SEM (Leo Gemini) before and after the EPOC experiments. The existence of FeO_x on the film surface has been proven by EDX. The pure Pt|YSZ system has been previously investigated by additional analytical techniques, including high resolution transmission electron microscopy (HRTEM) [36,37], pole figure analysis [36], X-ray and UV photoelectron emission microscopy (XPEEM, PEEM) [31,34], and CV [36]. The iron distribution of comparable Fe doped sample has been studied by EDX and TOF-SIMS (time of flight secondary ion mass spectrometry) [38].

2.3. EPOC measurements

The experimental setup has been described previously, e.g. in [3]. The atmospheric pressure single-chamber quartz reactor has a volume of 30 cm^3. Reactants were Messer Griesheim-certified standards of C_2H_4 in He and O_2 in He. They could be further diluted in ultrapure (99.999%) He (Air Liquide). The model-type reaction $C_2H_4 + 3O_2 \rightarrow 2CO_2 + 2H_2O$ was investigated. The gas composition ($p(O_2) = 8.2$ kPa, $p(C_2H_4) = 0.19$ kPa) was fixed and a flux of 210 ccSTP/min was adjusted. For analyzing the reactants a Beckman 864 IR CO_2 analyzer was used. Constant current or potentials were applied using an AMEL 553 galvanostat-potentiostat. All measurements were carried out between 553 K and 723 K, which is a temperature range where typically the maximum ρ values are obtained with Pt|YSZ catalysts [3]. In addition, this temperature range is much lower than the one used during the electrode preparation, which ensures that no temperature induced morphology changes appear. Firstly, the effect of temperature on the catalytic open-circuit rate r_o was investigated. Secondly, electrocatalytic measurements were carried out.

3. Results and discussion

3.1. Electrode characterization

3.1.1. Structure

XRD revealed a (1 1 1) orientation of all films parallel to the YSZ(1 1 1) surface (Fig. 1). For more detailed information on XRD of the un-doped Pt films including texture analysis we like to refer to a previous publication also showing high resolution [36] and analytical transmission electron microscopy (HRTEM) investigations of the Pt|YSZ interface [37]. Due to the small amount of Fe and the poor sensitivity of XRD a FeO_x phase could not be determined. The preparation by PLD always causes a variation of film thickness due to hardly controllable parameters, e.g. the non-uniform shape of the plasma plume, variation in the energy density of the laser on the target material due to focusing or the silvering of the passage window, or simply a slightly different target-substrate-laser geometry. Typical film thicknesses, as determined with the measurement of SIMS crater [38] or holes within the film (profilometer or atomic force microscopy, AFM) range between 200 nm and 1000 nm.

3.1.2. Impurities

The problem of inherent impurities within the electrode system is discussed in [35]. Due to unavoidable contaminations in the YSZ single crystals, we also find some impurities at the Pt|YSZ interface. However, their concentration is strongly reduced compared to the interface between a technical Pt paste and a commercial YSZ polycrystalline ceramic which contains different sintering aids. A detailed SIMS study of the Pt/FeO_x/Pt|YSZ system in dependency of temperature and electrochemical treatment showed a tendency of iron to segregate and accumulate at interfaces, i.e. at the interface Pt|YSZ and the Pt electrode surface [38]. Dark islands on the surface after annealing (cp. Fig. 2c, g, k, and n) were composed of iron oxide as proven by EDX. We did not determine the exact stoichiometry of the iron oxide, as it strongly depends on the experimental conditions, e.g. the oxygen activity in the course of electrochemical polarization, the sample temperature, the amount of iron segregation and the gas atmosphere. As these parameters vary during the experiment, only in situ characterization, e.g. high pressure XPS, would offer valid information.

3.1.3. Morphology

The surface morphology of the catalysts was studied by SEM after preparation and after the EPOC experiments. Before polarization the un-doped Pt films (Pt1, Pt2) covered the YSZ electrolyte. Except of some droplets caused by the preparation technique, the films had a smooth surface (left on Fig. 2a) and only an insignificant number of holes. The tpb of all samples was more or less jagged with some electrically disconnected Pt islands next to the tpb line,

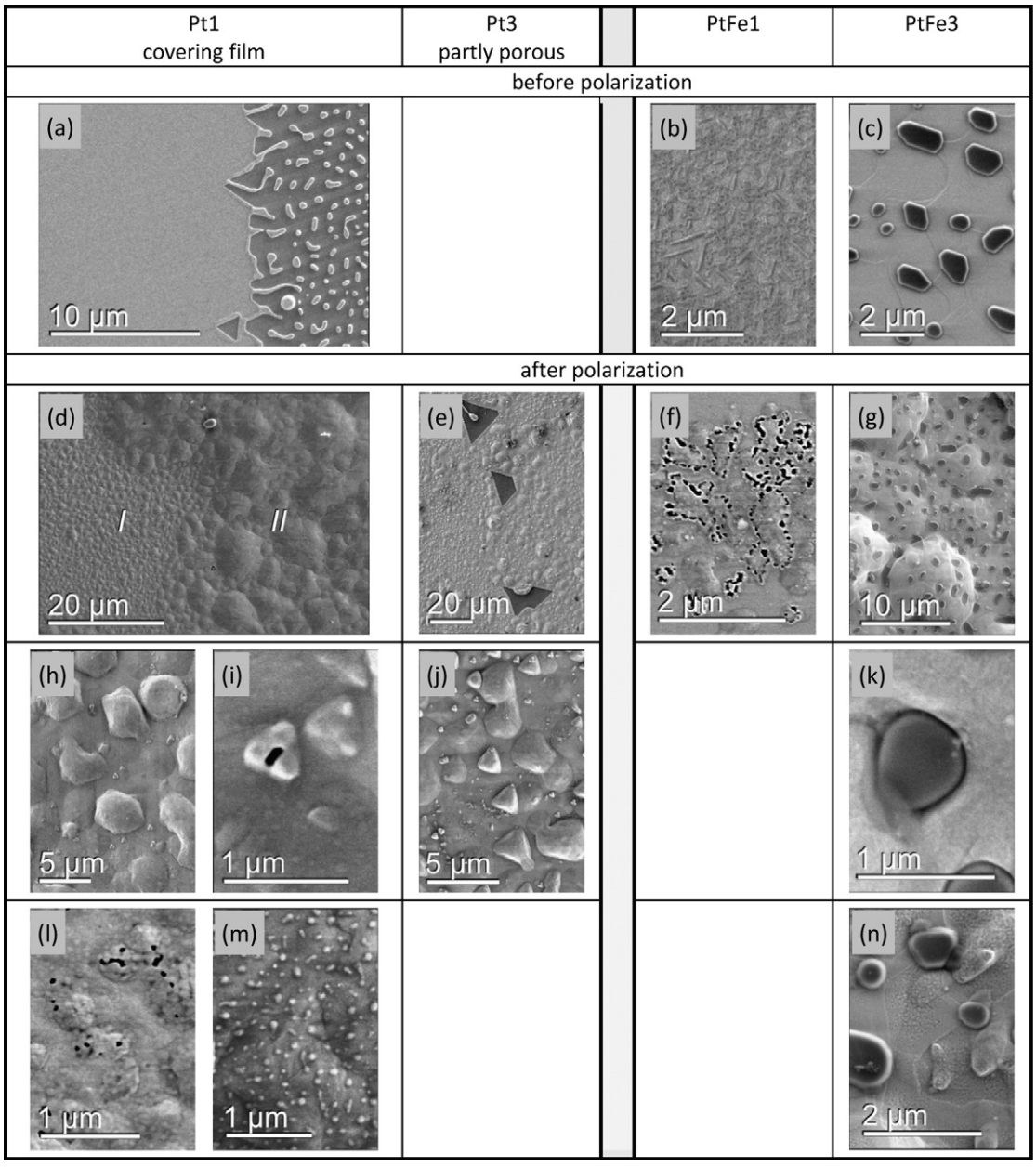

Fig. 2. SEM images of different catalyst films showing typical morphology changes due to the EPOC investigations. (a) tpb of a thin covering Pt film (Pt1) before EPOC, the darker areas represent YSZ; (b) and (c) iron-doped films before polarization (b = PtFe1, c = PtFe3). After EPOC: (d) two kinds of areas marked *I* and *II* (Pt1); (e) blistering at covering areas of the partly porous film Pt3; (g) geometrically less defined bubbles in the micrometer range (PtFe3); magnification of area *I*: (triangular shaped) bubbles in the micrometer and sub-micrometer range, (h) = Pt1, (j) = dense area of Pt3; (i) cracked triangular bubble in the sub-micrometer range in area *I* (Pt1); (k) gap between Pt and a FeO_x island (PtFe3); increased porosity next to the tpb of the (l) Pt1 film and (f) the PtFe1 catalyst; (m) area *II* with changed nanostructure (additional particles) of a Pt1 film, (n) formation of sub-micrometer bubbles and partially roughened surface structure (PtFe3).

as depicted in Fig. 2a. The covering iron-doped films (PtFe1–3) showed a different surface microstructure or the formation of iron oxide islands respectively (Fig. 2b and c). Note that the dark areas in the SEM images of sample PtFe3 (Fig. 2c, g, and n) represent iron containing islands while the darker areas shown in Fig. 2a, e, f, k, and l correspond to holes in the Pt film. The partly porous sample (Pt3) showed a few holes in the Pt film with dimensions in the micrometer range, as can be seen in Fig. 2e.

As expected, all film electrodes were morphologically unstable during the electrochemical experiments (Table 2). Two different kinds of changes appeared on most samples (Fig. 2d): areas with small distinct bubbles (marked *I*) and areas with large bubbles where the film was detached over more extended regions (marked *II*). However, we found no correlation between these two areas and any geometric quantity observable (e.g. distance to tpb, arrangement of the counter or reference electrode). The shape of the bubbles differed. In addition to these larger detachments (Fig. 2m), there were geometrically less defined bubbles in the micrometer range (Fig. 2e, h, and j) and small triangular shaped bubbles (Fig. 2h, i, and j) in the sub-micrometer range as previously observed [34]. A few of these smallest bubbles were cracked, which becomes apparent because of a dark point in the SEM image (Fig. 2i). Only on one sample (PtFe1) some of the micrometer sized bubbles were cracked. Even the partly porous catalyst film (Pt3) showed blistering in the covering areas as the number of holes in the electrode was too small to release the pressure build-up and prevent a bubble formation (Fig. 2e). In addition to the blistering, two other different phenomena took place: porosity of the film occurred in areas next to the tpb

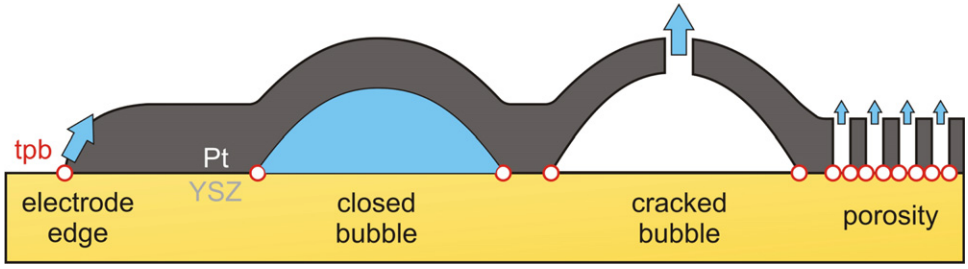

Fig. 3. Different morphological features of the film samples after electrochemical (anodic) polarization. The tpb is marked by small circles, the arrows indicate accessible tpb for reactants.

(Fig. 2f and l) and a change in the surface nanostructure appeared, i.e. an increased surface roughness (Fig. 2n) or the formation of small particles on the surface (Fig. 2i and m) respectively.

In general, a change of the electrode morphology can influence the Pt|YSZ|O_2 tpb length, and thus affect the generation of spillover oxygen and EPOC. Fig. 3 depicts the relevant morphologic features of the investigated thin film electrodes. Oxygen spillover diffusion starts from the red marked tpb, i.e. the edges of the electrode and bubbles or porous regions. However, regarding EPOC, solely catalyst areas contribute which are accessible for the reactants. Therefore, only the tpb at electrode edges, cracked bubbles and holes in the film has to be taken into account, while closed bubbles do not have to be considered.

As blistering took place at all samples, most of the bubbles did not crack and porosity only appeared in a region in vicinity to the electrode edges, the total increase of accessible tpb during the EPOC experiments is assumed to be small and comparable for all samples. Thus, we use the estimated tpb length values stated in Table 2 for the discussion.

As a direct influence of the morphology instabilities successively carried out EPOC experiments resulted in quantitatively slightly different results.

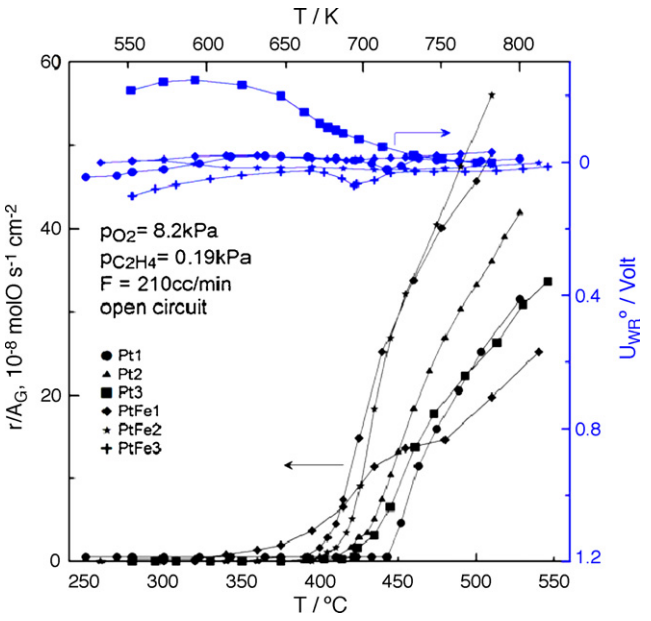

Fig. 4. Effect of temperature T on the open-circuit catalytic rate r_o and the open-circuit potential U^o_{WR} for all catalysts.

3.2. Open- and closed-circuit catalytic behavior

The onset of the open-circuit catalytic rate r was found between 673 K and 723 K (Fig. 4). Interestingly, the FeO_x-doped catalysts are more active at lower temperatures than the clean Pt catalysts. This is not too surprising in view of the early catalytic converter literature which shows that Fe_2O_3 is more active than Pt for light hydrocarbon and CO oxidation, but is much more susceptible to SO_2 poisoning [39]. It is interesting to note in Fig. 4 that the open-circuit potential, U^o_{WR}, of the partly porous Pt film (Pt3) is negative and significantly different from the others at temperatures below 730 K. This is similar to the behavior observed with typical porous metal films used in previous EPOC studies [3]. This negative potential has been interpreted to correspond via the Nernst equation to a low surface oxygen chemical potential or thermodynamic activity on the catalyst surface due to the depletion of chemisorbed oxygen by the catalytic reaction [3]. Thus, the U^o_{WR} behavior observed in Fig. 4 seems to imply that a minimum level of three-phase boundaries is necessary in order to establish the potential-setting reaction equilibrium at the tpb and thus allow for the use of the Nernst equation [3], and concomitant measurement of the low chemical potential of adsorbed oxygen on the catalyst surface.

Table 2
Summary of investigated samples, their EPOC behavior (type of EPOC, Lambda, Rho and Gamma values) and morphology changes after the EPOC experiments.

Notation	Type of EPOC	Lambda, Λ	Rho, ρ	Gamma, γ	Morphology	Morphology changes after the experiments
Pt1		No EPOC			Covering	Yes
Pt2		No EPOC			Covering	Marginal
Pt3	Reversible (648 K)/permanent (698 K)	−5.5/51 (648 K)	1.85/10.2 (648 K)	1	Partly porous	Yes (covering areas)
		32 (698 K)	4.3 (698 K)			
PtFe1	Permanent	37.7 (648 K)	55 (648 K)		Covering	Yes
PtFe2	Permanent	3.9 (648 K)	>10 (648 K)		Covering	
		6.7 (688 K)	2.1 (688 K)			Yes
		2.46 (723 K)	1.14 (723 K)			
PtFe3	Permanent	42/11 (648 K)	5.8/0.73 (648 K)	4.5	Covering	
		77 (698 K)	2.2 (698 K)			Yes

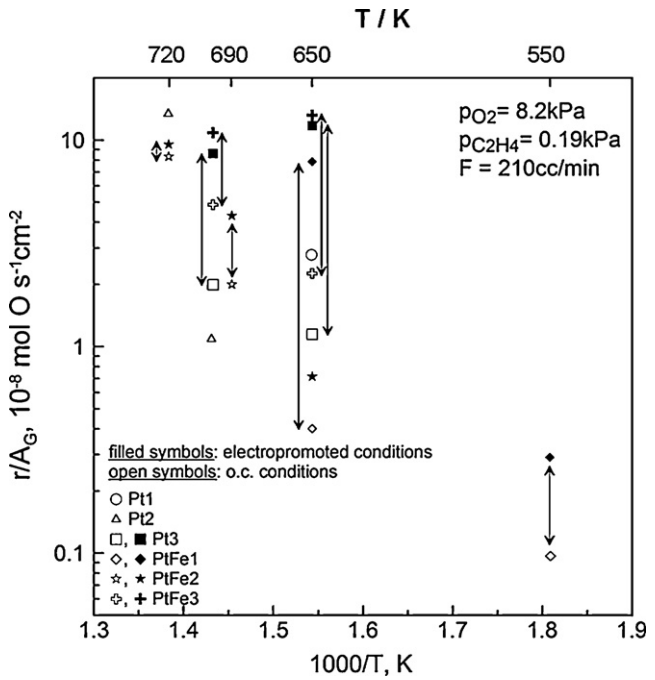

Fig. 5. Effect of temperature T on the unpromoted (open-circuit) and electropromoted specific rates r/A_G.

As shown in Fig. 5 the partly porous Pt(1 1 1) film (Pt3) and the PtFe samples showed EPOC with maximum effect observed at T = 648 K.

Table 2 sums up the observed type of EPOC (reversible or permanent) and the EPOC specification in terms of Lambda and Rho values for the investigated samples.

In general, the observed EPOC effect was smaller than the maximum one reported for the same reaction on porous Pt electrodes and polycrystalline YSZ ($\Lambda^{max} = 3 \times 10^5$, $\rho^{max} = 55$; $533 < T/K < 723$, cp. Appendix 2) [3]. The two covering Pt film catalysts without Fe did not show EPOC. The Rho and Lambda values obtained with the partly porous Pt film (Pt3) and the Pt/Fe films are similar. Furthermore only the partly porous catalyst (Pt3) showed reversible EPOC at 648 K and permanent EPOC at higher temperature (698 K). All investigated iron-doped samples exhibit permanent EPOC (P-EPOC).

3.2.1. EPOC with Pt(1 1 1)/YSZ(1 1 1) samples

The two covering Pt catalysts (Pt1, Pt2) did not show a measurable EPOC effect. The observed morphology changes (Fig. 2d, h, l, and m) visualize that oxygen was transported through the samples, thus excluding electrical contact problems during the measurements. The tpb of theses catalysts – mainly located at the edge of the electrode (Fig. 6a) – was estimated to be about 6 cm (cp. Table 1). For comparison a typically porous Pt paste electrode showing pronounced EPOC, has a much longer tpb. A microscopic observation of porous Pt paste electrodes on YSZ resulted in a tpb length of 0.5–22 m/cm^2 [40], corresponding to an about 50–200 times longer tpb. A simple geometric estimation and CV results lead to an even higher value of 235–315 m/cm^2 (about 2000–2700 times longer than the tpb length of the investigated covering samples) [41].

The results suggest that the area in which electrochemical polarization affects the catalytic reaction on the catalyst surface is limited only to the vicinity of this tpb. Fig. 6 depicts the suggested correlation between the tpb length of differently structured types of electrodes and the observed extent of EPOC. Such a dependency is consistent with the model for explaining EPOC [3–6].

In accordance with that trend, the partly porous Pt film electrode (Pt3) having a longer tpb (>193 cm) than the covering PLD films showed EPOC (Fig. 6b and 7).

At present little can be said about the actual size of this "vicinity". Its size must be dependent on temperature and gaseous composition but one may estimate from the SEMs of Fig. 7 that it is smaller than 10 μm since, as shown below, the electropromotion obtained with this film is modest (ρ = 10.2, Λ = 50) in comparison with that typically obtained with porous Pt paste films [3,5].

Fig. 7 shows galvanostatic transients of this sample obtained at 648 K and 698 K and SEM images of the catalyst film. At the lower temperature both positive and negative current enhanced the catalytic rate (inverted volcano behavior [3]) but the effect was more pronounced for positive current, i.e. the behavior is predominantly electrophobic. EPOC was reversible with ρ = 10.2 and Λ = 51. At the higher temperature the measurement was not long enough to decide whether a non-reversible EPOC behavior occurred or whether the relaxation took place on a different time scale. In addition, the transient showed an unexpected feature (around t = 15 min). The majority of observed transients for all samples showed the usual characteristics, as expected. A few measurements however resulted in different discontinuities. The reasons for these features are not yet understood.

Altogether, these results nicely demonstrate the crucial role of the tpb – as the starting point for the generation of spillover oxygen – for EPOC.

3.2.2. EPOC with Pt–FeO_x/YSZ(1 1 1) samples

The iron-doped samples showed EPOC (Table 2), which can be classified as P-EPOC according to the relaxation behavior. Fig. 8a depicts for instance galvanostatic transients obtained at 648 K with a covering Pt–Fe PLD film (PtFe3). The behavior was purely electrophobic, i.e. the rate increases with positive current (ρ = 5.6, Λ = 42) and decreased with decreasing current (ρ = 0.73, Λ = 11). It is worth noting the pronounced P-EPOC behavior with a γ value of 4.5. Similar was the behavior at higher temperatures (T = 698 K, Fig. 8b), although both γ (1.7) and ρ (2.2) decreased. Despite one exception (PtFe2 at 723 K, ρ = 1.14), we were unable to obtain any reversible EPOC behavior with the Pt–FeO_x/YSZ(1 1 1) catalysts. Fig. 8 also shows typical surface areas of the catalyst films before and after the experiment.

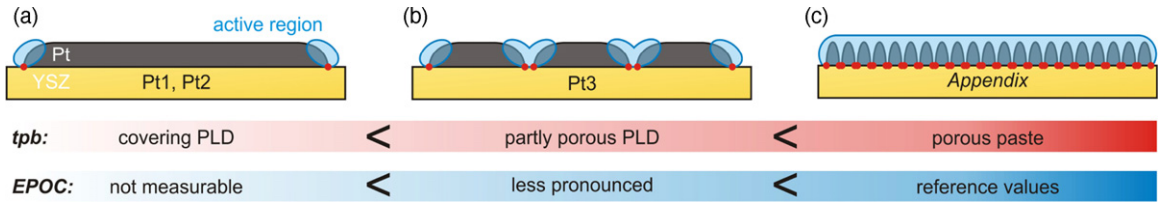

Fig. 6. Model for explaining the magnitude of observed EPOC by the tpb length, (a) covering PLD film, (b) partly porous PLD film, and (c) porous paste.

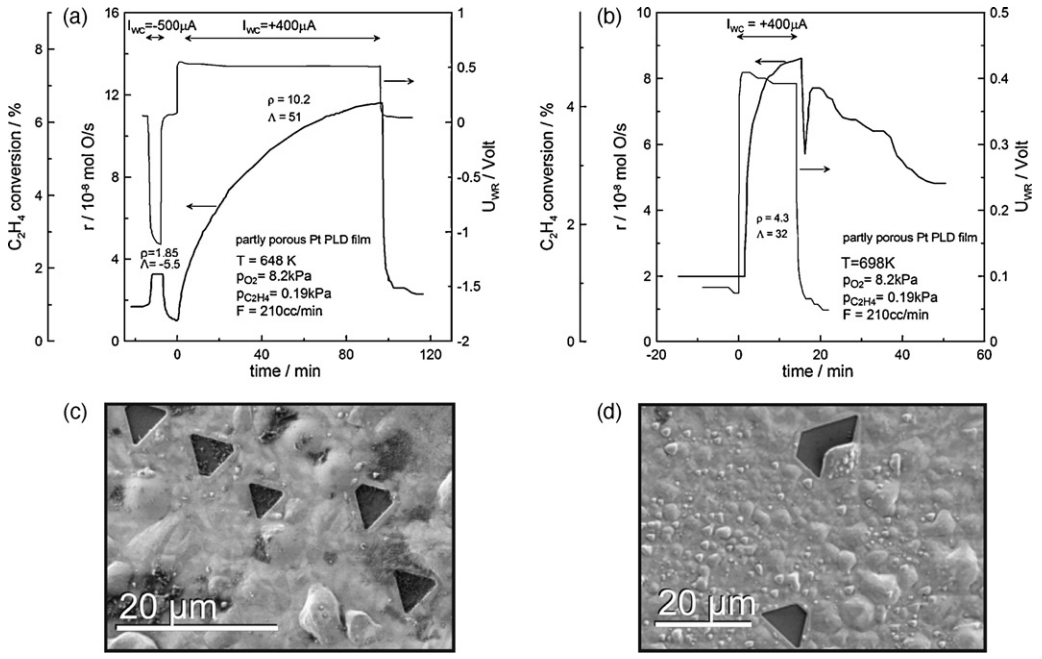

Fig. 7. Galvanostatic transient experiments for the partly porous Pt PLD film (Pt3) at (a) T = 648 K, (b) T = 698 K and (c, d) SEM images of the film after the electropromotion experiments (dark areas are holes).

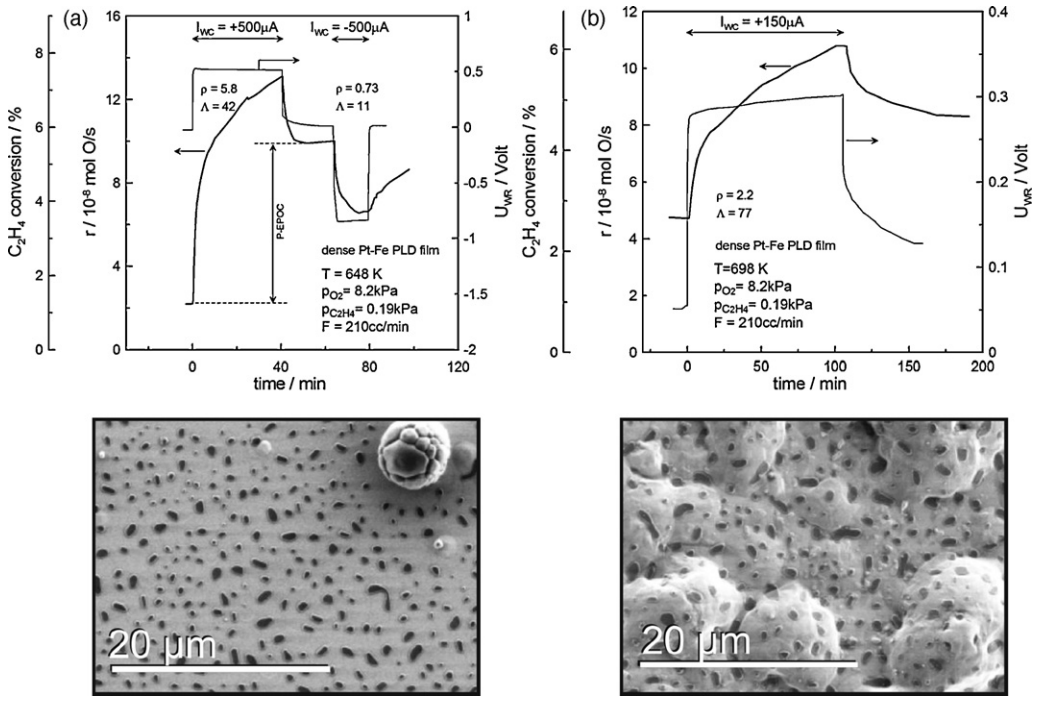

Fig. 8. Transient effect of imposed currents for the covering Pt–Fe catalyst (PtFe3) at (a) T = 648 K and (b) T = 698 K and SEM images of the catalyst film before (left) and after (right) the electropromotion experiments.

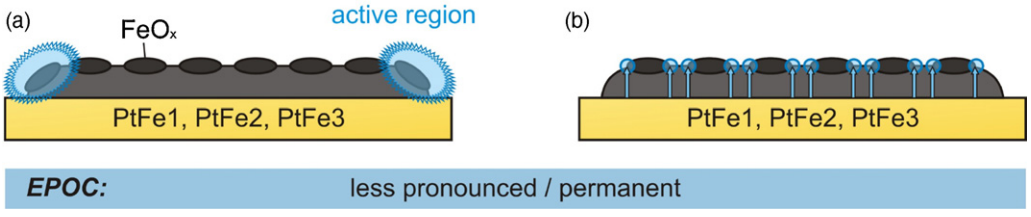

Fig. 9. Hypothetic model for explaining the influence of iron: (a) doping effect; (b) structural effect.

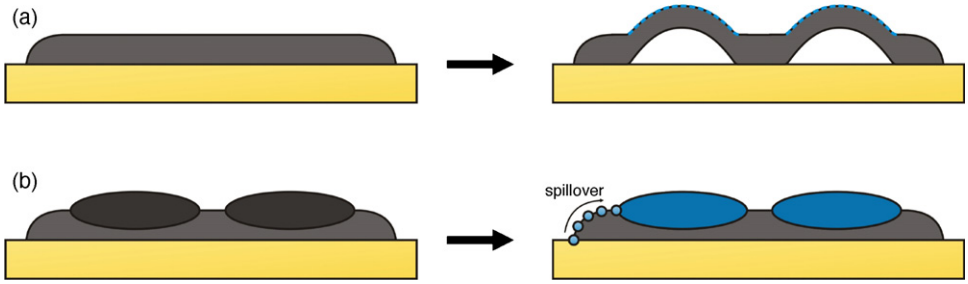

Fig. 10. Hypotheses for explaining the permanence of EPOC investigating thin film catalysts: (a) irreversible morphology change; (b) oxygen storage mechanism.

The conclusion that the tpb length affects the magnitude of EPOC appears not to be a sufficient explanation of the results: The estimated values of the tpb length for the covering iron-doped and un-doped Pt films are nearly identical (Table 1), but only the first ones exhibited an electropromotion effect. We can only hypothesize about the reasons or additional influencing parameters. Fig. 9 depicts two potential explanations:

On the one hand, the surface iron doping might influence the active region (Fig. 9a). An enhanced electropromotion could be caused by a laterally more extended active region, e.g. due a different diffusion coefficient of the spillover species on Pt and iron-doped material or a different desorption rate of the spillover species into the gas phase. A higher catalytic activity of the active region could also account for the observation. Oxygen spillover diffusion on iron-doped Pt might lead to a different change of the catalytic properties compared to iron-free Pt. Varying the oxygen potential during electrochemical polarization can lead to a change of the oxidation state of iron. Surface iron oxides might have a higher catalytic activity.

On the other hand, a structural effect might be the reason for observing EPOC. While the covering un-doped films are nearly single crystalline [36], we assume to find an increased number of grain boundaries in the iron-doped films, e.g. at the edges of the iron oxide islands (Fig. 2l shows a small chink between an iron oxide island and the Pt film after polarization). The blistering during electrochemical polarization (Fig. 2h) indicated the high gas-tightness of the films. However, in addition a slow oxygen diffusion along grain boundaries within the film might take place. In this case anodic polarization would cause small active regions on the electrode surface, as depicted in Fig. 9b.

Based on our results, we cannot distinguish between both hypothetical cases and it is quite possible that both play a role interfering with each other. Further work will be focused on clarifying this point, e.g. in situ spectroscopic investigations of the oxidation state of iron during EPOC or the investigation of a polycrystalline Pt film without iron doping will be useful.

3.3. Permanent EPOC effect of iron-doped films

The iron-doped samples showed permanent EPOC (P-EPOC) with γ values between 1.7 and 10. Thus, the presence of iron appears to play a role. This agrees with the observation that the partly porous sample without iron showed a reversible EPOC effect at low temperature. As this sample revealed a complex (non-reversible) relaxation behavior at higher temperature, other reasons might also influence the permanence of EPOC. At this point, we like to offer two possible explanations for the P-EPOC (Fig. 10). Again, for detailed insights further investigations are necessary.

Firstly, bubble formation is an irreversible morphology change and therefore can be a reason for a permanent phenomenon (Fig. 10a). Once the built up oxygen pressure underneath the catalyst film caused a plastic deformation, the original situation will not be recovered. In principle, a changed morphology may alter the catalytic properties of a metal film, e.g. due to the appearance of atomic steps, differently orientated surfaces or the generation of structural defects. However, the bubble formation seems to play a subordinate role.

Secondly, the results suggest a contribution of Fe/FeO_x additives. In the case of reversible EPOC, upon switching off the potential the catalytic active species is consumed quickly and by this the initial rate r_0 is restored. Iron oxide, FeO_x, might act as a reservoir for the promoting oxygen species, e.g. by forming a catalytically active iron oxide with a higher oxidation state (Fig. 10b). After stopping the polarization the iron oxide might be more stable compared to the quickly consumed spillover oxygen.

4. Conclusions

Our study demonstrates that Pt thin film model catalysts Pt(1 1 1)/YSZ(1 1 1) prepared by PLD – which offer the chance to carry out in situ studies using surface science techniques – exhibit reversible EPOC if they have a sufficient tpb length. Not surprisingly, Pt(1 1 1) catalyst films on YSZ(1 1 1) single crystals with a minimum tpb show no measurable EPOC.

Thus, the extent of the observed reversible EPOC can be explained by morphology, i.e. mainly the length of the tpb. Its important role as the location where spillover oxygen is generated becomes apparent.

Interestingly, iron-doped covering Pt films lead to P-EPOC. This was unexpected, since iron-free covering films show no measurable EPOC effect. The origin of this difference is yet unclear. Our hypothesis is that the presence of iron/iron oxide dopants either influences the microstructure or acts as a reservoir for oxygen.

Also interestingly, similar Λ and ρ values were observed for the iron-doped and covering films (P-EPOC) and for the iron-free and porous films (reversible EPOC). These results cannot be explained yet and require additional work.

Acknowledgements

The Giessen group is grateful for financial support to the German Research Foundation (project Ja 648/10-1). E.M. and J.J. thank for the hospitality of the Patras group during visits and E.M. for the opportunity to join EPOC experiments in Patras. We all thank our reviewers for helpful comments and suggestions.

Appendix 1. Catalyst–electrode preparation techniques used for EP studies

	Catalyst–electrode preparation	Catalyst–electrode/ electrolyte system	Reaction under study	ρ	$\lvert\Lambda\rvert$	Ref.
1a	Sputtering Rh and Pt on YSZ plates Rh and Au on YSZ plates	Rh/YSZ/Pt and Rh/YSZ/Au	Ethylene oxidation NO reduction by ethylene	1.45 NO: 1.33 CO_2: 1.44	77 1.65 27	[21]
1b	Sputtering Ir-deposited on YSZ	Ir/YSZ	NO reduction with propene	N_2 yield 38–64% Propene conversion 47–60%	Ir-40-HP N_2: 570 C_3H_6: 66	[22]
2a	Impregnation Pt film preparation by thermal decomposition of a H_2PtCl_6 solution	Pt-Au/YSZ	Ethylene oxidation	3	704	[23]
2b	Impregnation Pt film preparation by thermal decomposition of a H_2PtCl_6 solution	Pt/K-β″-Al_2O_3	CO oxidation	Up to 11		[25]
2b	Impregnation Pt film preparation by thermal decomposition of a H_2PtCl_6 solution	Pt/Na–β″-Al_2O_3	NO reduction by propene	NO: 1.4	–	[24]
2c	Nitrate impregnation $AgNO_3$ deposition on YSZ	Ag/YSZ	Toluene oxidation	1.6	−13,000	[26]
3	Spray deposition in C matrix Pt/C film via spraying on K-β″-Al_2O_3	Pt-C/K-β″-Al_2O_3	CO and C_3H_6 oxidation	CO: 1.2 C_3H_6: 4.8		[30]
4	Electrostatic spray deposition Pt films deposition by ESD on YSZ, $Pt(NH_3)_4(OH)_2(H_2O)$ or $Pt(acac)_2$	Pt/YSZ	NO reduction by propene	N_2: 2.0 CO_2: 2.3	48	[29]
5a	Thermal decomposition technique Ir precursor deposition on YSZ	IrO_2/YSZ	Ethylene oxidation	2.6		[28]
5b	Ru precursor deposition on YSZ	RuO_2/YSZ	Ethylene oxidation toluene oxidation	11 8	170 12	[27]
6a	Calcination of unfluxed organometallic pastes (Pt paste A1121, Engelhardt)	Pt/YSZ	Ethylene oxidation	55	3×10^5	[3]

Appendix 2. Electrochemical promotion (EP) studies of C_2H_4 oxidation on Pt

Electron donor (D)	Electron acceptor (A)	Products	Catalyst	Solid electrolyte	T (°C)	Λ_{max} (>0) or Λ_{min} (<0)	ρ_{max} (>1) or ρ_{min} (<1)	PI_O^{2-}	Ref.
C_2H_4	O_2	CO_2	Pt	YSZ	260–450	3×10^5	55	55	[3]
C_2H_4	O_2	CO_2	Pt	TiO_2 (TiO_x^+, O^{2-})	450–600	5×10^3	20	20	[3]
C_2H_4	O_2	CO_2	Pt	CeO_2 (CeO_x^+, O^{2-})	500	-10^5	3	–	[42]
C_2H_4	O_2	CO_2	Pt	YZTi 10	400–475	−250	2	–	[43]
C_2H_4	O_2	CO_2	Pt	β″-Al_2O_3	180–300	5×10^4	0.25	−30	[3]
C_2H_4	O_2	CO_2	Pt	$Na_3Zr_2Si_2PO_{12}$	430	–	10	300	[44]
C_2H_4	O_2	CO_2	Pt	$CaZr_{0.9}In_{0.1}O_{3-a}$	385–470	-3×10^4	5	–	[45]

References

[1] M. Stoukides, C.G. Vayenas, J. Catal. 70 (1981) 137.
[2] C.G. Vayenas, S. Bebelis, S. Ladas, Nature 343 (1990) 625.
[3] C.G. Vayenas, S. Bebelis, C. Pliangos, S. Brosda, D. Tsiplakides, Electrochemical Activation of Catalysis: Promotion, Electrochemical Promotion and Metal–Support Interactions, Kluwer Academic, New York, 2001.
[4] R. Lambert, in: A. Wieckowski, E.R. Savinova, C.G. Vayenas (Eds.), Catalysis and Electrocatalysis at Nanoparticle Surfaces, Marcel Dekker, Inc., New York, 2003.
[5] C.G. Vayenas, C.G. Koutsodontis, J. Chem. Phys. 128 (2008) 182506.
[6] A. Katsaounis, J. Appl. Electrochem. 40 (2010) 885–902.
[7] S.G. Neophytides, C.G. Vayenas, J. Phys. Chem. 99 (1995) 17063.
[8] A. Jaccoud, G. Fóti, C. Comninellis, Electrochim. Acta 51 (2006) 1264–1273.
[9] D. Kek, M. Mogensen, S. Pejovnik, J. Electrochem. Soc. 148 (2001) A878.
[10] S. Ladas, S. Kennou, S. Bebelis, C.G. Vayenas, J. Phys. Chem. 97 (1993) 8845.
[11] W. Zipprich, H.-D. Wiemhöfer, U. Vöhrer, W. Göpel, Ber. Bunsenges. Phys. Chem. 99 (1995) 1406.
[12] B. Luerssen, S. Günther, H. Marbach, M. Kiskinova, J. Janek, R. Imbihl, Chem. Phys. Lett. 316 (2000) 331.
[13] X. Li, F. Gaillard, P. Vernoux, Top. Catal. 44 (2007) 391.
[14] J. Poppe, A. Schaak, J. Janek, R. Imbihl, Ber. Bunsenges. Phys. Chem. 102 (1998) 1019.
[15] B. Luerssen, E. Mutoro, H. Fischer, S. Günther, R. Imbihl, J. Janek, Angew. Chem. Int. Ed. 45 (2006) 1473.
[16] C.G. Vayenas, D. Archonta, D. Tsiplakides, J. Electroanal. Chem. 554–555 (2003) 301.
[17] J. Janek, M. Rohnke, B. Luerssen, R. Imbihl, PCCP 2 (2000) 1935–1941.
[18] G. Pacchioni, F. Illas, S. Neophytides, C.G. Vayenas, J. Phys. Chem. 100 (1996) 16653.
[19] E.P.M. Leiva, C. Vanquez, M.I. Rojas, M.M. Mariscal, J. Appl. Electrochem. 38 (2008) 1065–1073.
[20] C. Falgairette, A. Jaccoud, G. Fóti, C. Comninellis, J. Appl. Electrochem. 38 (2008) 1075–1082.
[21] S. Balomenou, D. Tsiplakides, A. Katsaounis, S. Thiemann-Handler, B. Cramer, G. Foti, Ch. Comninellis, C.G. Vayenas, Appl. Catal. B: Environ. 52 (3) (2004) 181–196.
[22] P. Vernoux, F. Gaillard, R. Karoum, A. Billard, Appl. Catal. B: Environ. 731 (2) (2007) 73–83.
[23] M. Marwood, C.G. Vayenas, J. Catal. 178 (1998) 429–440.
[24] F. Dorado, A. de Lucas-Consuegra, P. Vernoux, J.L. Valverde, Appl. Catal. B: Environ. 73 (2007) 42–50.
[25] A. de Lucas-Consuegra, F. Dorado, J.L. Valverde, R. Karoum, P. Vernoux, Catal. Commun. 9 (1) (2008) 17–20.
[26] F. Gaillard, N. Li, Catal. Today 146 (3–4) (2009) 345–350.
[27] Ch. Comninellis, G.P. Vercesi, J. Appl. Electrochem. 21 (1991) 136–142.
[28] I. Constantinou, I. Bolzonella, C. Piangos, Ch. Comninellis, C.G. Vayenas, Catal. Lett. 100 (3–4) (2005) 125.
[29] A. Lintanf, E. Djurado, P. Vernoux, Solid State Ionics 178 (39–40) (2008) 1998–2008.
[30] A. de Lucas-Consuegra, A. Princivalle, A. Caravaca, F. Dorado, A. Marouf, C. Guizard, J.L. Valverde, P. Vernoux, Appl. Catal. A: Gen. 365 (2) (2009) 274–280.
[31] J. Janek, B. Luerßen, E. Mutoro, H. Fischer, S. Günther, Top. Catal. 44 (2007) 399–407.
[32] E. Mutoro, B. Luerßen, S. Günther, J. Janek, Solid State Ionics 179 (2008) 1214–1218.
[33] A. Gurlo, R. Riedel, In Situ and Operando Spectroscopy for Assessing Mechanisms of Gas Sensing, Angew. Chem. Int. Ed. 46 (2007) 3826–3848.
[34] E. Mutoro, S. Günther, B. Luerßen, I. Valov, J. Janek, Solid State Ionics 179 (2008) 1835–1848.
[35] E. Mutoro, B. Luerßen, S. Günther, J. Janek, Solid State Ionics 180 (2009) 1019–1033.
[36] G. Beck, H. Fischer, E. Mutoro, V. Srot, K. Petrikowski, E. Tchernychova, M. Wuttig, M. Rühle, B. Luerßen, J. Janek, Solid State Ionics 178 (2007) 327–337.
[37] V. Srot, M. Watanabe, C. Scheu, P.A. van Ake, E. Mutoro, J. Janek, M. Rühle, Analytical TEM Investigations of Pt|YSZ Interfaces, EMC 2008, vol. 2: Materials Science, Springer-Verlag, Berlin, Heidelberg, 2008, pp. 369–370.

[38] H. Pöpke, Diploma Thesis, JLU Giessen.;
E. Mutoro, N. Baumann, J. Janek, J. Phys. Chem. Lett. 1 (2010) 2322.
[39] H.H. Voge, C.R. Adams, Adv. Catal. 17 (1967) 151.
[40] T. Kenjo, Y. Yamakoshi, K. Wada, J. Electrochem. Soc. 140 (1993) 2151.
[41] C.G. Vayenas, A. Ioannides, S. Bebelis, J. Catal. 129 (1991) 67–87.
[42] P.D. Petrolekas, S. Balomenou, C.G. Vayenas, J. Electrochem. Soc. 145 (1998) 1202.
[43] P. Beatrice, C. Pliangos, W.L. Worrell, C.G. Vayenas, Solid State Ionics 136/137 (2000) 833.
[44] P.D. Petrolekas, S. Brosda, C.G. Vayenas, J. Electrochem. Soc. 145 (4) (1998) 1469.
[45] M. Makri, A. Buekenhoudt, J. Luyten, C.G. Vayenas, Ionics 2 (1996) 282.